POLITECNICO DI TORINO
Repository ISTITUZIONALE

Magnetic Model Self-Identification for PM Synchronous Machine Drives

Publisher copyright

(Article begins on next page)

05 August 2020

Magnetic Model Self-Identification for PM Synchronous Machine Drives

Gianmario Pellegrino[1], Barbara Boazzo[1], Thomas M. Jahns[2]

1. Politecnico di Torino,
2. University of Wisconsin – Madison

gianmario.pellegrino@polito.it, barbara.boazzo@polito.it, jahns@engr.wisc.ed

Abstract: **The Magnetic Model Self-Identification of PM Synchronous machines is proposed and experimentally validated. Provided that the shaft is free to turn, the commissioning procedure consists of spinning the machine to positive and negative speed values by way of an appropriate pattern of dq current reference values. The flux linkage versus current curves of the machine are constructed during the test via the standard measurements available on any industrial drive: phase currents, dc-link voltage and shaft position. Respect to the literature, the proposed method does not require a specific test rig nor off-line mathematical manipulation.**

I. INTRODUCTION

The world of Permanent Magnet (PM) synchronous machines spans a very wide range of sizes and uses. Recent key electrification applications such as traction, green energy conversion, and more-electric aircraft make use of high-density PM machines of different types, including both salient-pole Interior PM (IPM) and Surface-mounted PM (SPM) machines that are designed to operate with high levels of magnetic saturation [1-3]. All such machines have a nonlinear magnetic model, intended as the relationship between the current vector and the flux linkage vector, normally represented in the *dq* frame synchronous to the rotor. Whatever the salient or non-salient nature of the machine, when saturation is involved the magnetic model is expressed in the very general form of flux linkage tables [4]:

$$\begin{cases} \lambda_d = \lambda_d\big(i_d, i_q\big) \\ \lambda_q = \lambda_q\big(i_d, i_q\big) \end{cases} \qquad (1)$$

Where both the flux linkage components are a function of both the current components.

The accurate identification of the magnetic model (1) is a nontrivial effort, and it is of primary importance both for design verification and control purposes. In the literature the magnetic model of synchronous machines was identified via finite element analysis [4], blocked rotor tests [5], constant speed tests [6-9] or inspection of the machine impedance via the injection of high frequency signals [10]. All methods have their advantages and limitations. FEA simulations are not always accurate enough, and they must be eventually validated by experiments. Locked rotor tests can determine the current-generated flux components, but not the PM flux linkage. Constant speed tests need for specific extra hardware including a speed-controlled prime mover, sometimes a Wattmeter, the measurement of pulse-width modulated machine voltages, etc.. according to the adopted technique.

This paper presents a magnetic model self-identification (MMSI) technique that can be preliminarily performed at the first drive start-up with no need for extra hardware. The MMSI procedure evaluates the *dq* flux linkages comprehensively, including the PM flux linkage, saturation and cross saturation, and in a very short time, i.e. with a negligible perturbation of the PM temperature. The machine can be driven by its same inverter, with the shaft left free, and current controlled. The output of the commissioning procedure are two flux linkage tables, one for the *d*- and one for the *q*- flux components, in the form of (1). The tables can be readily used for control purposes: in flux-observer implementations [11-13], where the flux linkage estimate from the magnetic model covers the low speed operating region, and in sensorless control, for compensation of the position error caused by cross-saturation [4,20-22]. Besides, the curves manipulation can lead to the accurate determination of the machine control trajectories and the machine final performance [4,9]. The method is useful to make custom-designed machines controllable by third parts, so to open new opportunities to the diffusion of this class of machines.

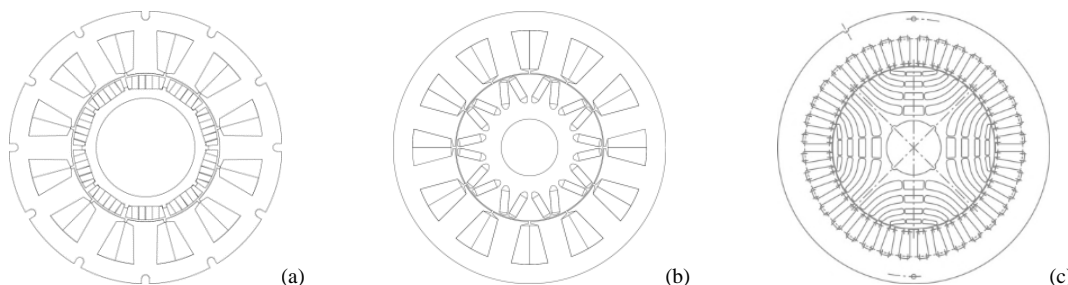Three PM synchronous machines (..) are tested for the validation of the proposed MMSI procedure.

Figure 1.   PM traction machines tested in this investigation. a) Surface Mounted PM with concentrated windings (SPM); b) Interior PM with concentrated windings (IPM); c) PM-assisted Synchronous Reluctance machine with distributed windings (PM-SyR).

Their cross-sections are in Fig. 1 and their ratings are reported in Table I, in Section III. The first two machines have the same stator, with concentrated windings (CW), combined once with a Surface Mounted PM (SPM) rotor and then with an Interior PM (IPM) rotor. The third machine is a PM-assisted Synchronous Reluctance (PM-SyR) machine with distributed windings. Experimental results are provided for the three machines. All three machines are for traction, but as said the method applies to all PM synchronous machine drives, regardless of the application.

II. MAGNETIC MODEL SELF-IDENTIFICATION

The shaft is free and the machines are self-accelerated and decelerated by way of the closed loop current vector control according to a determined pattern of vector current references $(i_d{}^*, i_q{}^*)$. The values of the terminal voltages are estimated via the references signals output by the current vector controller. The position sensor (e.g. encoder) individuates the dq synchronous coordinates. Speed is derived by time differentiation of the position measurement. The proportional-integral (PI) current regulators are tuned according to constant estimates of the dq machine inductances. Back-emf cross coupling terms are feedback compensated by the PI regulators, since model-based feed-forward compensation is not possible prior to the machine identification.

A. Flux Linkage Maps in the dq Current Plane

The dq flux linkages tables form (1) is preferred to the inductance-based approach very often used in the literature because includes all saturation and cross-saturation effects, and does not need for the segregation of the PM-flux linkage term, which is embedded into the tables (1). From the flux linkage curves the machine torque can be calculated with precision in any operating point, e. g. with the flux linkage – MMF approach [14] or simply as the external vector product of the flux linkage and current vectors:

$$T = \tfrac{3}{2} p \cdot \left(\lambda_d\, i_q - \lambda_q\, i_d \right) \qquad (2)$$

Where p is the number of pole pairs and the flux components are obtained by interpolation of the experimental look-up tables (1). The magnetic curves are identified over a regularly spaced grid of points in the dq current domain, having the form of a rectangular mesh as in Fig. 2. The second quadrant of the current plane is the only one considered in the figure.
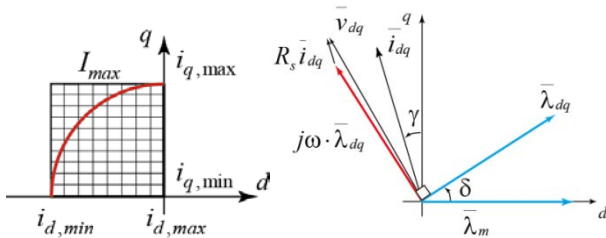

Figure 2.   a) Sample current plane of a PM synchronous machine illustrating the type of current vector grid used for the MMSI identification procedure; b) steady-state vector diagram of a PM synchronous machine.

The first and forth quadrants (the d-current enforces the PMs) are out of interest during closed-loop operation and the 3rd

quadrant is obtained from the 2nd, by symmetry. The current domain is rectangular here for the sake of simplicity. In real self-commissioning applications, the converter current limit I_{max} must be respected, as evidenced in Fig. 2a. In these cases, the area of identification can be usefully reorganized in the form of a polar coordinates mesh, with current amplitude varying from 0 to I_{max} and current phase angle stepping from zero to 90 degrees.

B. Flux Linkage Estimation Principle

As said, the shaft of the machine under test is disconnected from any non-inertial load. Starting from zero speed, the set-points $(i_d{}^*, i_q{}^*)$ are imposed to the current vector controller and the machine accelerates.

The fixed (i_d, i_q) condition corresponds to a steady torque value and then to a speed ramp at constant acceleration. During this period also the flux linkage vector is steady, in dq coordinates. So there is a time interval when the dq flux linkage vector components can be derived from the back-emf estimate, also in dq coordinates. Under the assumption of constant dq flux linkage it is possible to drop the flux derivative term from the voltage equation as shown in (3):

$$\bar{v}_{dq} = R_s \bar{\imath}_{dq} + \frac{d\bar{\lambda}_{dq}}{dt} + j\omega \bar{\lambda}_{dq} = R_s \bar{\imath}_{dq} + j\omega(t) \cdot \bar{\lambda}_{dq} \quad (3)$$

Where $\omega(t)$ is the electrical speed which is ramping up or down, R_s is the stator resistance and v_d, v_q are the voltage vector components. The assumption (3) is strictly true only after the current components (i_d, i_q) have reached their set-point, i.e. after the very short initial electrical transient.

The flux linkage can be estimated from the machine terminal voltages and currents in dq coordinates via the simple formulas:

$$\lambda_d = \frac{v_q(t) - R_s i_q}{\omega(t)} \qquad \lambda_q = -\frac{v_d(t) - R_s i_d}{\omega(t)} \qquad (4)$$

The formulas (3) and (4) are graphically represented by the vector diagram in Fig. 2b. The time-dependence recalls that the speed varies during the test, and the voltage signals along with it.

Returning to (4), the speed information is derived from the shaft position sensor and the voltage vector comes from the voltage commands, after the inverter error component is accurately compensated. Also the stator resistance value must be known and compensated. Those three aspects are discussed later in this section.

Fig. 3 reports the example of a slow MMSI speed ramp, obtained with the IPM machine under test controlled at $i_d = -100$ A, $i_q = 20$ A and with additional inertia. The measured speed and the dq currents are reported. The estimated fluxes (4) are repeatedly calculated at all sampling time instances by the real-time controller, starting from 400 rpm and ending at the maximum target speed of 800 rpm. After the final speed is reached, all the occurrences of (4) collected in the 400 rpm to 800 rpm speed window are eventually averaged, to produce the final dq flux linkage estimates at $i_d = -100$ A, $i_q = 20$ A.
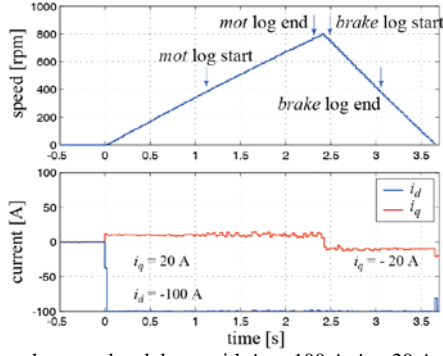
Figure 3. Speed ramp ud and down with i_d = -100 A, i_q = 20 A and i_q reversal at 800 rpm. The data log window in the example is between 400 rpm and 800 rpm.
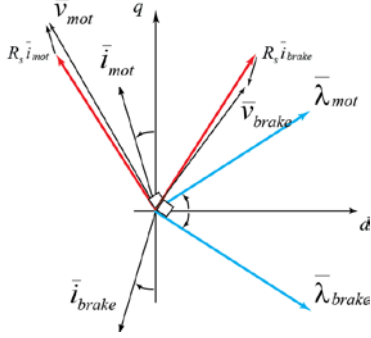

Figure 4. Steady state vector diagram in dual motoring and braking conditions.

C. Motor-Brake Average

At the reach of the maximum speed the i_q component is reversed and the machine decelerates. In Fig. 3 the dual current condition (i_d, -i_q) is used for deceleration, because this gives the opportunity to estimate the flux linkage a second time in a symmetrical condition. The two steady state vector situations are represented in Fig. 4 and indicated, respectively, with *mot* and *brake*. The flux linkage vector is identical in the two cases, apart from the sign of the q component. During the deceleration the flux is estimated again via (4) with the same accumulate and average procedure and in the same speed window. At the end of one up and down cycle the *mot* and *brake* flux linkage estimates are averaged (5).

$$\lambda_d = \frac{\lambda_{d,mot} + \lambda_{d,brake}}{2} \qquad \lambda_q = \frac{\lambda_{q,mot} - \lambda_{q,brake}}{2} \qquad (5)$$

The mot-brake average reduces the effect of residual non compensated errors of the machine estimated voltage and series resistance.

D. Example of Current and Speed Waveforms

A sequence of (i_d, i_q) current couples is shown in Fig. 5 for the SPM machine example. The i_d is initially set to -100A and the i_q starts from 10A, it is reversed every time the speed reaches its target and progressively incremented in absolute value up to a final value of 100 A. Tests at positive and negative speed are alternated, as a countermeasure against an incorrect setting of the encoder offset, as explained in subsection II.K. Once i_q is cycled from 10 A to 100 A, the i_d reference switches to the next value of -80 A and i_q that restarts from 10 A, and so on.
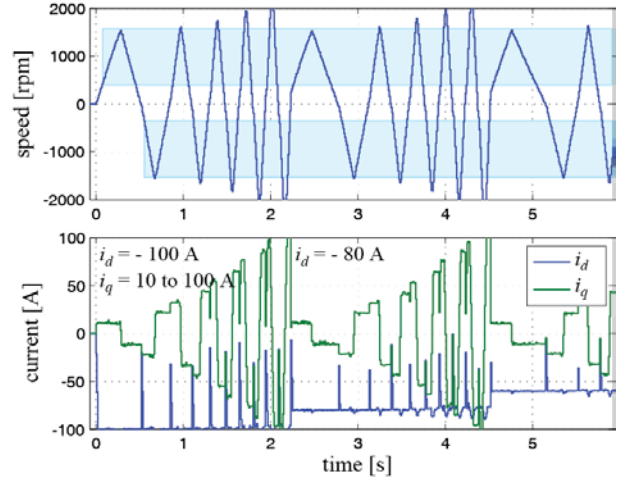

Figure 5. Speed and *dq* current waveforms during the MMSI. The current pattern is i_d from -100 A to 0 A, i_q from 10 A to 100 A, both with step 10 A.

E. Stator Resistance and Inverter Identification

The stator resistance and the inverter voltage error are identified and compensated with the off-line direct-current procedure described in [15]. Other techniques are also effective [16]. The off-line procedure is embedded into the drive control software. Also the inverter identification is run once, whereas the stator resistance must be estimated every time prior to utilize the MSSI procedure, to account for the actual machine temperature. It is assumed that the machine temperature does not vary during the MMSI procedure, that is normally rather quick. If otherwise, the R_s identification can be repeated from time to time during the MMSI routine.

The R_s and inverter identification sequence is shown in Fig. 6a, referring to the IPM machine example, and consisting of a sequence of dc current pulses imposed by the current controller.
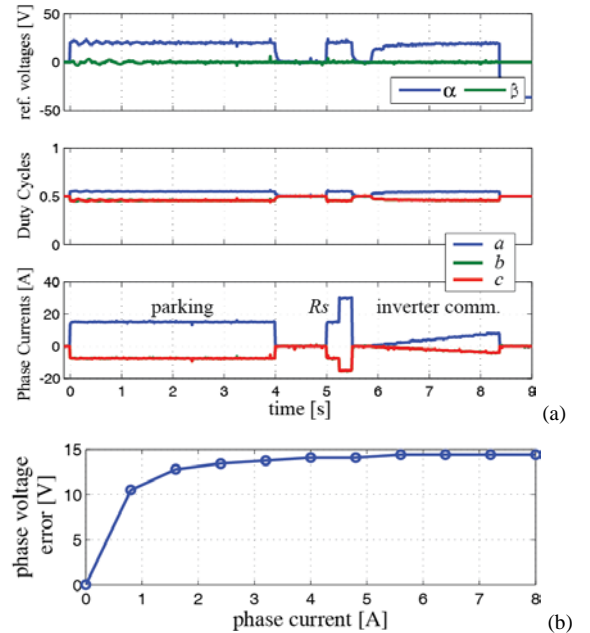

Figure 6. a) Inverter error identification sequence: 1) parking, 2) R_s identification, 3) inverter compensation commissioning. b) Current to voltage look-up table for inverter error compensation.

In the *parking* stage a dc current commanded along the stator *alpha* axis aligns the *d-* rotor axis to its position zero. Two dc current pulses commanded along *d-* are used for the measurement of the stator resistance. Finally, the table of values for the compensation of the non-linear inverter error is obtained as a function of the phase current by imposing a staircase of dc current steps, once again along the *d-* axis. The resulting inverter look-up table is represented in Fig. 6b.

F. Filtering of the Speed Quantization Noise

In all the experiments of this paper the speed signal was derived from the position signal measured by incremental encoders. The encoders of the IPM and SPM machines have 1024 optical divisions and the encoder of the PM-SyR machine has 512 divisions. The speed signal derived from the encoder position (6) is quantized and thus chattering, as shown in Fig. 7:

$$\omega_k = \frac{sin(\vartheta_k)\,cos(\vartheta_{k-1}) - cos(\vartheta_k)\,sin(\vartheta_{k-1})}{T_s} \quad (6)$$

Where T_s is the sampling period. The electrical position increment $\theta_k - \theta_{k-1}$ between the present (k) and the previous ($k-1$) time instants is approximated by the cross products of the angle sines and cosines for avoiding the discontinuity occurring at the encoder index.
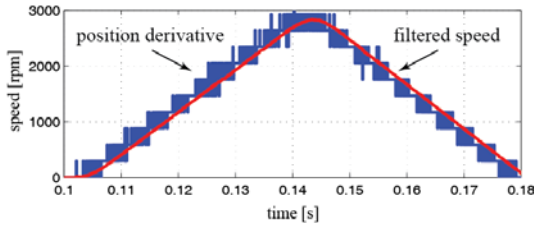

Figure 7.   Speed signal derived by the encoder position: time derivative (blue) and speed signal filtered with a 50 Hz 1st order filter (red).

The quantized time derivative (6) must be filtered for all closed loop control purposes [17]. However, a standard filter delays the measured speed signal with respect to the actual speed, as shown in Fig. 7. Such delay is not acceptable here for flux linkage estimation at variable speed. It is in fact mandatory that the current, voltage and speed samples in (4) are perfectly synchronized at all times, and that the speed value is the actual one.
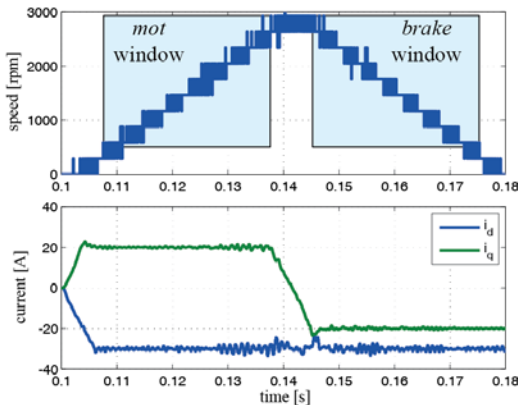

Figure 8.   Test of the PM-SyR machine at i_d = -30 A, i_q = 20 A and i_q reversal at 3000 rpm. Top) Non-filtered speed signal and effect of the encoder quantization; bottom) *dq* current waveforms.

Fig. 7 shows that the speed measurement, when filtered, is constantly lagging and then it underestimates the actual speed during the acceleration ramp and overestimates it during the deceleration, producing flux linkage misestimates of opposite signs if applied to (4). A velocity observer could eliminate the noise and improve the dynamics of the filtered speed signal [17]. However, in the spirit of offering a calibration-free commissioning technique to the industry, the speed signal used here is the plain, non-filtered time derivative of the encoder position signal.

In Fig. 8 the log of the non-filtered speed signal is shown, during the MMSI sequence of the PM-SyR test machine. The sampling frequency is 10 kHz, set by the pulse-width modulation (PWM) of the inverter. With 512 divisions, 10 kHz and p = 2, the speed noise is 61.3 rad/s, or 293 rpm, peak to peak:

$$\Delta\omega = 2 \cdot \frac{2\pi}{4 \cdot 512} \cdot 10\,[kHz] = 61.\,3\,[rad/s] \quad (7)$$

With a chattery speed signal like the one in Fig. 8 the flux estimate samples (4) are very noisy. The noise is eliminated by averaging a large number of samples over the speed window. It is then important that the speed window is chosen, as addressed in subsection II.J.

G. Torque Estimation

During the execution of the MMSI procedure, the machine torque at each (i_d, i_q) test is estimated in real-time via equation (2), and an additional torque LUT is built. This additional results can be of use for many purposes, both in post-processing and in real-time. For example, the maximum torque per Ampere and per Volt trajectories can be readily evaluated from the torque contours, associated to the current and flux linkage contours. In Fig. 9 the MMSI-estimated torque contours of the PM-SyR machine under test are reported, and compared with the corresponding measured torque.

The bold lines, self-identified in the restricted area i_d = -30A – 0A, i_q = 4A – 20A, are perfectly superimposed to the thin lines of the measured torque values, referring to a broader current area. The torque measurements in Fig. 9 come from a specific test, not reported in the paper.
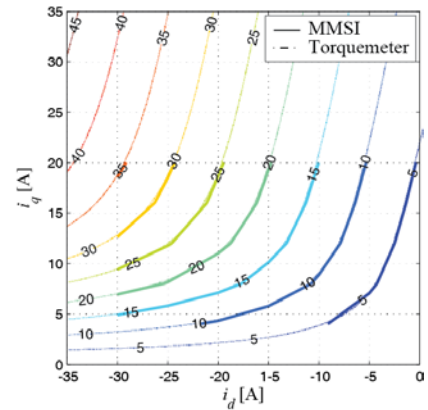

Figure 9.   Torque contours in the *dq* current plane: comparison between the measured values and the MMSI estimated values.

4

The machine under test was run at low speed by a dc machine via a reduction gear and the torque is measured by means of a torque-meter at all vector current conditions. The inverter used at the time of the torque-meter tests had a larger current rating.

H. Inertia Estimation

The torque estimate is also useful to derive the total moment of inertia, according to:

$$J_{est} = T_{est} \frac{\Delta t}{|\omega_{max} - \omega_{min}|} \qquad (7)$$

Where T_{est} is the just estimated torque value, ω_{max} and ω_{min} [mech. rad/s] are the start and the end speed values used for data collection, and Δt is the time interval between the two speed marks, measured by the real-time controller. The inertia estimate, repeated at all (i_d, i_q) points of the MMSI procedure can usefully indicate if the flux linkage identification is proceeding correctly: the estimated inertia is expected to be the same at all points of the current plane. Two examples are shown in Fig. 10, for the IPM machine alone and for the SPM machine with the additional inertia of the dynamometer motor. By way of the inertia estimate (7) it is possible to build automated check procedures for evaluating the success of the entire MMSI session or single points of it.

I. No Torque Area

One limitation of the proposed MMSI technique is the impossibility of identification in the no torque regions of the dq current plane, such as area around the d-axis ($i_q = 0$). With null or little torque there are no acceleration and deceleration.

Strictly speaking, this means that the magnetic LUTs from the MMSI will miss one row, as represented in Fig. 11 and remarked in the comments to the experimental results at section III.
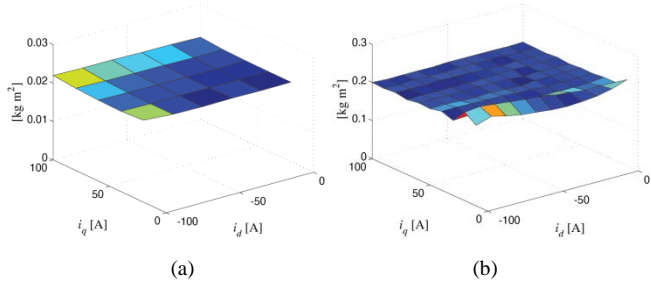

(a)   (b)

Figure 10. Moment of inertia, estimated during the MMSI. a) IPM machine only; b) SPM machine, coupled with the dynamometer motor.
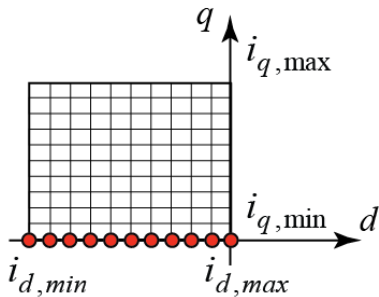

Figure 11. No-torque area in the current vector grid used for the MMSI identification procedure.

In practical terms, this is a minor issue because the no torque conditions have little importance during operation. Nevertheless, the flux linkage tables must be completed to avoid numerical discontinuities in their use, either for direct implementation into a flux observer [10-11], or for post processing purposes.

Dealing with the q-flux linkage table, a practical way to extrapolate the missing values is to assume that the flux is zero at zero i_q, which is no approximation. Dealing with the missing $\lambda_d(i_d, 0)$ curve, this can be replaced by doubling the next one $\lambda_d(i_d, i_{q,min})$, where $i_{q,min}$ is 10 A for the SPM and IPM machines and 4 A for the PM-SyR machine in the experiments at Section III. This coarse approximation showed to be effective when tested with model-based predictive control of the kind of [10-11], which would be very chattery in case of model imprecisions and was not, for all three machines. Other approaches are possible for a more accurate extrapolation of the missing data $\lambda_d(i_d, 0)$, like imposing the conservation of the stored magnetic energy [4], but they require post-processing and gave no practical benefit, for the machines under test.

J. Selection of the Target Speed

The top speed of the MMSI procedure must take into account the effect of speed-dependent losses, like iron and PM losses. If the speed is high to the point that such losses are not negligible, then the controlled (i_d, i_q) currents are no longer representative of the sole magnetizing current, but contain an equivalent iron loss current component, which distorts the flux linkage to measured currents relationship. It is not easy to formulate a general rule valid for all possible machines under identification. An inherent limitation to the test speed comes from the limited inverter voltage. Translated in terms of speed, it means that the target speed is necessarily lower than the corner speed, because of the voltage limit. Furthermore, a speed margin is needed, for including the current overload conditions where duty-cycle saturation occurs below the corner speed. In a way, the voltage limit preserves from wrong speed choices and heavy distortions due to iron and PM loss. Specific cases can suggest to reduce the speed further, e.g. for machines with a high number of poles and a high rated frequency. In uncertain cases the suggestion is to repeat the MMSI procedure at different final speeds and compare the results for checking their consistency.

K. Position sensor offset

The propagation of encoder offset errors is prevented by alternating positive and negative speed values over the (i_d, i_q) grid as represented in the example of Fig. 5. If the encoder offset was incorrect then the final flux look-up tables would be evidently irregular, since the points coming from the positive speed tests would all show over- or under-estimated flux linkage values and vice-versa. Such error check and eventual corrective actions can be easily automatized, but this is out of the scope of this paper.

L. PM Temperature

The PM temperature is not perturbed during the MMSI session due to its short duration. One complete MMSI

sequence can take from less than one minute to some minutes, according to 1) the torque/inertia ratio of the machine under test, 2) the selected target speed and 3) the number of (i_d, i_q) test points. It is very easy to have the magnetic curves at room temperature, running the MMSI procedure at cold conditions. If needed, the machine can be warmed at a willed operating temperature prior to run the MMSI procedure. To the authors' experience, what is very important is that the PM temperature is constant during the identification and that this temperature reasonably known. In this context, the quickness of the MMSI method is one of its key benefits.

III. EXPERIMENTAL RESULTS

A. Machines Under Test

The cross-sections of the three prototype machines under test are illustrated in Fig. 1. The concentrated-winding IPM and SPM machines [18] are both rated for 55 kW (peak) and 30 kW continuous power, with a maximum rotor speed of 14000 rpm and a corner speed of 2800 rpm, in accordance with the specifications of the FreedomCar 2020 powertrain. They have a common stator and replaceable rotors. The rotor switch operation is documented in Fig. 12. The ends of the concentrated windings and the pipes for liquid cooling are also visible in the figures.
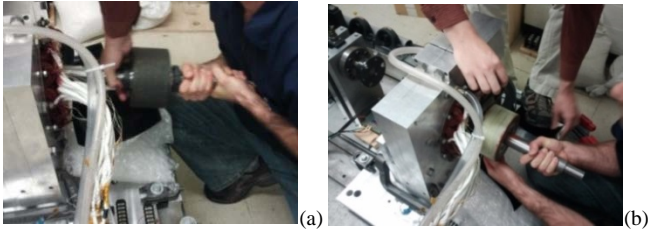

(a)   (b)

Figure 12. Switching from the IPM (a) to the SPM (b) rotor for the concentrated-winding machines of [16].

The PM-assisted synchronous reluctance machine is similar to the one reported in [20], rated 7 kW (continuous), with a maximum speed of 10000 rpm and a corner speed of 2450 rpm. Its pictures are reported in Fig. 13. The main ratings of the three machines are in Table I.
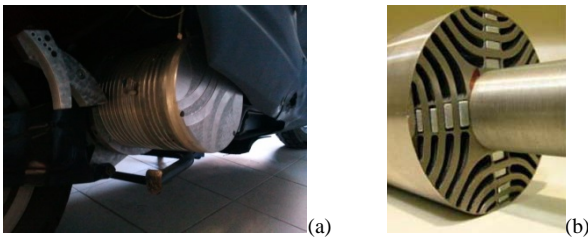

(a)   (b)

Figure 13. Pictures of the PM-assisted Synchronous Reluctance machine used in the tests. a) Bottom view of the scooter, the aluminum housing of the motor is visible. b) View of the rotor stack and shaft.

B. Experimental Setups

The experiments have been run on two different test rigs. The two concentrated winding IPM and SPM machines have the same experimental setup and were tested in the same conditions on the test bed represented in Fig. 14. This is equipped with a dSPACE 1103 PPC Controller board. Both rotors have encoders with 1024 divisions and the switching and

sampling frequency is 8 kHz. The second test rig is used for the PM-SyR machine. Its picture is reported in Fig. 15 and it is very similar to the previous one. The real-time processor is a dSPACE 1104 R&D Controller board in this case. The encoder of the PM-SyR machine has 512 divisions and the sampling frequency is 10 kHz.

Figure 14. Setup #1, used for the IPM and the SPM machines. The dSPACE 1103 PPC host computer is on the desk. The machine under test is in the red square at the bottom right corner, connected to an induction machine dyno via a torque-meter (not visible). Power converters are in the other square on the left hand corner.

Figure 15. Setup #2. The dSPACE 1104 R&D host computer is visible on the desk. The PM-SyR machine under test and the inverter are in the red squares.

TABLE I. MAIN RATINGS OF THE THREE MACHINES UNDER COMPARISON

	IPM	SPM	PM-SyR
Number of slots	12		36
Pole pairs (p)	5		2
Stator outer diameter	274		150
Stack length [mm]	73.4		142
Airgap [mm]	0.73	1.85	0.3
Rated speed [rpm]	2800		2450
Rated Torque [Nm]	102		27
Rated current [Apk]	113	109	28
Characteristic current [Apk]	50	87	14
Dc-link voltage [V]	320	320	400
Open-circuit voltage line to line [Vpk]	314	328	60
Inertia [kg m²]	$21 \cdot 10^{-3}$	$21 \cdot 10^{-3}$	$4.3 \cdot 10^{-3}$
Type of cooling	liquid		natural ventilation

6

C. Experimental Magnetic Curves

The proposed MMSI procedure was applied to the three machine examples in different conditions, as summarized in Table II.

The IPM and SPM machines were identified with the dynamometer machine turned off but still coupled to their shafts, i.e. with a large additional inertia. The total inertia is about ten times the one of the machine alone (199 kg·m² versus 21 kg·m²). This relented the accelerations and eased the numerical filtering of the speed quantization because a large number of speed samples was easily collected even with a limited target speed (1000 rpm). After this first sessions of tests, the dynamometer motor was decoupled and the IPM and SPM machines were identified with no additional inertia. In this second test campaign the very quick speed response suggested to double the top speed to 2000 rpm to obtain a sufficient number of samples. The top speed is lower than the corner speed for staying clear from iron loss and maximum voltage limit, as said. The duration of the tests in this second test campaign was below 30 sec. There is no appreciable difference between the curves taken with augmented inertia and without.

Fig. 16 reports the flux linkage curves of the IPM machine in the domain $i_d =$ -100 A to 0, $i_q =$ 10 A to 100 A, obtained with the MMSI procedure with no additional inertia. According to the curves, the d- and q- inductances show no substantial difference, despite of the anisotropic IPM rotor structure. This to say that a minor reluctance torque contribution is expected from this machine. Cross-saturation effects are evident in the figure. The analogous curves are reported for the SPM machine in Fig. 17. The open circuit flux linkage (d-flux at zero current) is very close to the one of Fig. 16, as also reported in Table I.

TABLE II. MIN AND MAX SPEED SETTINGS USED IN THE MMSI TESTS

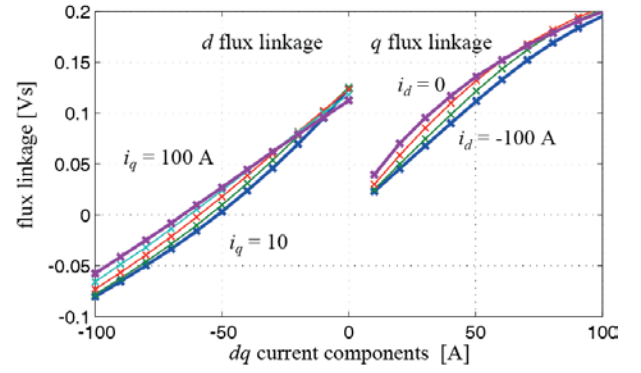|		IPM & SPM	PM-SyR
Free shaft	Min speed [rpm]	500	500
	Max speed [rpm]	2000	2200
	Min time window [ms]	33	25.5
	Min number of samples [ms]	264	255
Additional Inertia (0.199kg·m² total)	Min speed [rpm]	400	/
	Max speed [rpm]	1000	/
	Min time window [ms]	83.4	/
	Min number of samples	686	/

Figure 16. Flux curves of the IPM machine example, obtained with the proposed MMSI technique.
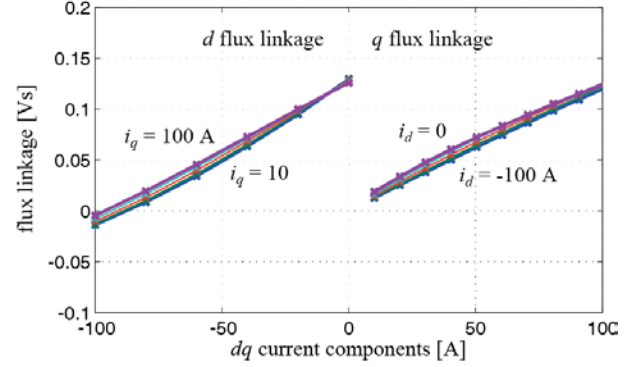

Figure 17. Flux curves of the SPM machine example, obtained with the proposed MMSI technique
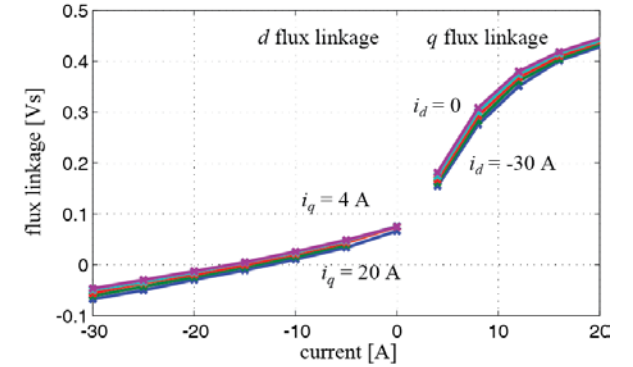

Figure 18. Flux curves of the PM-SyR machine example, obtained with the proposed MMSI technique.

The slopes of the d- and q- flux linkage curves are very close to each other, accounting for the non-salient nature of the machine. From the comparison with Fig. 16 it is also clear that the dq inductances of the SPM machine are lower than the corresponding inductances of the IPM machine having the same stator. This is expected, from the larger total airgap (air plus magnets) of the former one. The cross saturation in Fig. 17 is also much reduced, again due to the thicker air-gap.

The MMSI tests for the PM-SyR machine were run at free shaft, with a top speed of 2200 rpm. The PM-SyR machine curves are represented in Fig. 18, showing the typical shape expected from a PM-assisted machine: the q- flux linkage is the main flux component and the PM flux linkage is very small if compared to it. The q- flux linkage curves resemble the

magnetization curves of a SyR machine. Cross saturation is limited, as for the SPM machine.

Figure 19.

D. Comparison with the constant speed identification

The results of the MMSI procedure are compared to the flux linkage curves obtained a constant-speed, dynamometer motor driven method [9]. The constant speed test results are reported for the IPM and SPM motors in Figs. 19 and 20, respectively, showing a very good agreement with the results of the MMSI.
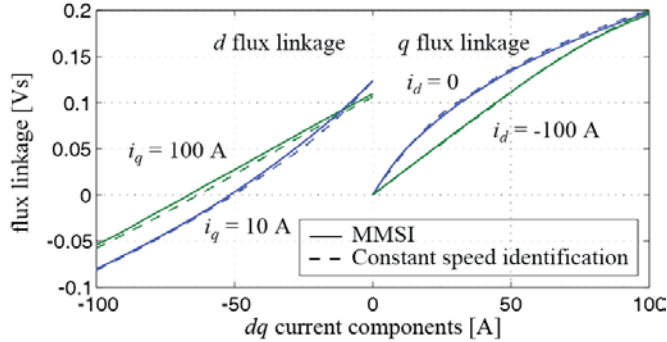

Figure 20. Flux linkage curves obtained with the presented MMSI procedure (continuus lines) and with the constant speed technique of [9] (dashed lines) for the IPM machine example.
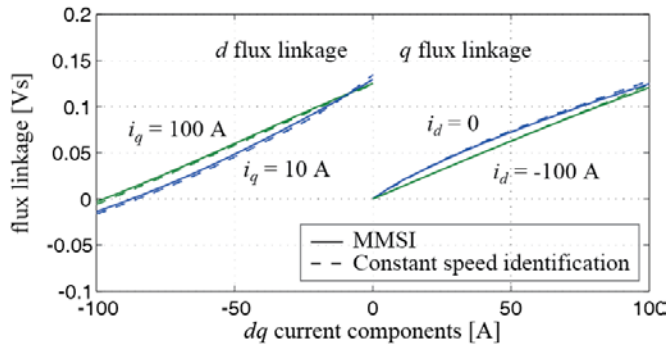

Figure 21. Flux linkage curves obtained with the presented MMSI procedure (continuous lines) and with the constant speed technique of [9] (dashed lines) for the SPM machine example.

IV. DISCUSSION

The key features of the presented MMSI method are:
1) includes all magnetic aspects comprehensively (PM-flux linkage, saturation, cross saturation);
2) it is stand-alone, no specific test facilities are required;
3) it is embedded into the drive control firmware;
4) it is quick, so that it can be added to the drive installation routine. Plus, the PM temperature is not perturbed during the tests;
5) it is self-adjustable: the inertia estimate and the use of both positive and negative speeds provide valuable feedback for the automatic recalibration of the encoder offset and the MMSI parameters.

V. CONCLUSION

The paper demonstrates the feasibility and the effectiveness of a new magnetic model self-identification method, applicable to any PM synchronous machines with no need for hardware modifications.

The paper explains how to implement and calibrate the method in detail, for the sake of industrial application.

Other than the flux linkage tables, the method can estimate the output torque map and the moment of inertia of the machine under test.

The experimental results, produced for three machine examples, have been compared with the ones obtained with one method in the literature and with the torque measurements by a torque-meter, showing to be extremely accurate.

The results of the MMSI procedure are the flux linkage and torque tables, that are directly applicable to control implementation, or can be usefully manipulated for the definition of the machine ratings or for modelling purposes.

REFERENCES

[1] EL-Refaie, A. M. , "Fractional-Slot Concentrated-Windings Synchronous Permanent Magnet Machines: Opportunities and Challenges," Industrial Electronics, IEEE Transactions on , vol. 57, no. 1, pp. 107,121, Jan. 2010

[2] Jahns, T. M. , "The expanding role of PM machines in direct-drive applications," Electrical Machines and Systems (ICEMS), 2011 International Conference on , vol. , no. , pp. 1,6, 20-23 Aug. 2011

[3] Rahman, K. ; Jurkovic, S. ; Stancu, C. ; Morgante, J. ; Savagian, P. , "Design and performance of electrical propulsion system of extended range electric vehicle (EREV) Chevrolet Voltec," Energy Conversion Congress & Expo (ECCE), 2012 IEEE , pp. 4152-4159, Sept. 2012

[4] N. Bianchi and S. Bolognani "Magnetic models of saturated interior permanent magnet motors based on finite element analysis", Conf. Rec. IEEE IAS Annu. Meeting, vol. 1, pp. 27 -34 1998

[5] B. Stumberger , G. Stumberger , D. Dolinar , A. Hamler and M. Trlep "Evaluation of saturation and cross-magnetization effects in interior permanent-magnet synchronous motor", IEEE Trans. Ind. Appl. , vol. 39, no. 5, pp. 1264 -1271 2003

[6] Nee, H-P; Lefevre, L. ; Thelin, Peter; Soulard, J. , "Determination of d and q reactances of permanent-magnet synchronous motors without measurements of the rotor position," Industry Applications, IEEE Transactions on , vol. 36, no. 5, pp. 1330,1335, Sep/Oct 2000

[7] K. Rahman and S. Hiti "Identification of machine parameters of a synchronous motor", IEEE Trans. Ind. Appl. , vol. 41, no. 2, pp. 557 -565 2005

[8] R. Dutta and M. Rahman "A comparative analysis of two test methods of measuring d- and q-axes inductances of interior permanent-magnet machine", IEEE Trans. Magn. , vol. 42, no. 11, pp. 3712 -3718 2006

[9] Armando, E. ; Bojoi, R. I. ; Guglielmi, P. ; Pellegrino, G. ; Pastorelli, M., "Experimental Identification of the Magnetic Model of Synchronous Machines," Industry Applications, IEEE Transactions on, vol. 49, no. 5, pp. 2116,2125, Sept. -Oct. 2013

[10] Wei Xu; Lorenz, R. D. , "High frequency injection-based stator flux linkage and torque estimation for DB-DTFC implementation on IPMSMs considering cross-saturation effects," Energy Conversion Congress and Exposition (ECCE), 2013 IEEE , pp. 844,851, 15-19 Sept. 2013

[11] Boazzo, B. ; Pellegrino, G. , "Predictive direct flux vector control of Permanent Magnet Synchronous Motor drives," Energy Conversion Congress and Exposition (ECCE), 2013 IEEE , pp. 2086-2093, 15-19 Sept. 2013.

[12] Jae Suk Lee; Chan-Hee Choi; Jul-Ki Seok; Lorenz, R. D. , "Deadbeat-Direct Torque and Flux Control of Interior Permanent Magnet Synchronous Machines With Discrete Time Stator Current and Stator Flux Linkage Observer," Industry Applications, IEEE Transactions on , vol. 47, no. 4, pp. 1749,1758, July-Aug. 2011.

[13] Boldea, I. ; Paicu, M. C. ; Andreescu, G. ; Blaabjerg, F. , ""Active Flux" DTFC-SVM Sensorless Control of IPMSM," Energy Conversion, IEEE Transactions on , vol. 24, no. 2, pp. 314,322, June 2009.

[14] Staton, D. A. ; Deodhar, R. P. ; Soong, W. L. ; Miller, T. J E, "Torque prediction using the flux-MMF diagram in AC, DC, and reluctance

motors," Industry Applications, IEEE Transactions on , vol. 32, no. 1, pp. 180,188, Jan/Feb 1996

[15] Pellegrino, G. ; Bojoi, R. I. ; Guglielmi, P. ; Cupertino, F. , "Accurate Inverter Error Compensation and Related Self-Commissioning Scheme in Sensorless Induction Motor Drives," Industry Applications, IEEE Transactions on , vol. 46, no. 5, pp. 1970,1978, Sept. -Oct. 2010

[16] Jong-Woo Choi; Seung-Ki Sul, "Inverter output voltage synthesis using novel dead time compensation," Power Electronics, IEEE Transactions on , vol. 11, no. 2, pp. 221,227, Mar 1996

[17] Lorenz, R. D. ; Van Patten, K. W. , "High-resolution velocity estimation for all-digital, AC servo drives," Industry Applications, IEEE Transactions on , vol. 27, no. 4, pp. 701,705, Jul/Aug 1991

[18] Reddy, P. B. ; EL-Refaie, A. M. ; Kum-Kang Huh; Tangudu, J. K. ; Jahns, T. M. , "Comparison of Interior and Surface PM Machines Equipped With Fractional-Slot Concentrated Windings for Hybrid Traction Applications," Energy Conversion, IEEE Transactions on , vol. 27, no. 3, pp. 593,602, Sept. 2012

[19] Pellegrino, G. ; Armando, E. ; Guglielmi, P. , "Direct Flux Field-Oriented Control of IPM Drives With Variable DC Link in the Field-Weakening Region," Industry Applications, IEEE Transactions on , vol. 45, no. 5, pp. 1619,1627, Sept. -oct. 2009

[20] Guglielmi, P.; Pastorelli, M.; Vagati, A., "Impact of cross-saturation in sensorless control of transverse-laminated synchronous reluctance motors," *Industrial Electronics, IEEE Transactions on* , vol.53, no.2, pp.429,439, April 2006

[21] Reigosa, D.D.; Garcia, P.; Raca, D.; Briz, F.; Lorenz, R.D., "Measurement and Adaptive Decoupling of Cross-Saturation Effects and Secondary Saliencies in Sensorless Controlled IPM Synchronous Machines," Industry Applications, IEEE Transactions on , vol.44, no.6, pp.1758,1767, Nov.-dec. 2008

[22] Zhu, Z.Q.; Gong, L.M., "Investigation of Effectiveness of Sensorless Operation in Carrier-Signal-Injection-Based Sensorless-Control Methods," Industrial Electronics, IEEE Transactions on , vol.58, no.8, pp.3431,3439, Aug. 2011